Interfacial roughening in nonideal fluids: Dynamic scaling in the weak- and strong-damping regime

Markus Gross[1,*] and Fathollah Varnik[1,2]
[1]*Interdisciplinary Centre for Advanced Materials Simulation (ICAMS), Ruhr-Universität Bochum, Universitätsstr. 90a, 44789 Bochum, Germany*
[2]*Max-Planck Institut für Eisenforschung, Max-Planck Str. 1, 40237 Düsseldorf, Germany*
(Received 2 October 2012; published 25 February 2013)

Interfacial roughening denotes the nonequilibrium process by which an initially flat interface reaches its equilibrium state, characterized by the presence of thermally excited capillary waves. Roughening of fluid interfaces has been first analyzed by Flekkoy and Rothman [Phys. Rev. Lett. **75**, 260 (1995)], where the dynamic scaling exponents in the weakly damped case in two dimensions were found to agree with the Kardar-Parisi-Zhang universality class. We extend this work by taking into account also the strong-damping regime and perform extensive fluctuating hydrodynamics simulations in two dimensions using the Lattice Boltzmann method. We show that the dynamic scaling behavior is different in the weakly and strongly damped case.

DOI: 10.1103/PhysRevE.87.022407 PACS number(s): 68.03.Kn, 05.40.−a, 47.11.−j, 47.35.Pq

I. INTRODUCTION

Capillary fluctuations on an interface between two fluid phases are waves that are excited by thermal noise in the bulk [1–7]. From a macroscopic viewpoint, capillary fluctuations make the interface "rough" and increase the effective interface width. Roughening of interfaces is a fundamental aspect of nonequilibrium dynamics and has been widely studied in the literature (see, e.g., Refs. [8–12] for reviews). Most models for interface growth, such as the Edwards-Wilkinson [13] or Kardar-Parisi-Zhang [14] equations, describe a purely local growth mechanism. In the case of an interface between two fluids, however, one can expect significant dynamical effects arising from the coupling of the order parameter to the hydrodynamic flow field. Indeed, as has been shown in Refs. [15,16], the effective Langevin description of a roughening fluid interface is in general non-Markovian due to the surrounding flow. The roughening of fluid interfaces due to thermal fluctuations is potentially relevant for the stability of patterns that form, for instance, in reaction-diffusion systems [17,18] or during phase-transitions under shear [19–22]. Also, coalescence of droplets or films [23] or the dynamics of wetting transitions [24] are potentially affected by interfacial roughening.

Thermal roughening of fluid interfaces was first studied in Refs. [15,16] based on the equations of fluctuating hydrodynamics and by simulations of an immiscible lattice gas (see also Ref. [25] for the same problem in the presence of surfactants). There, it was concluded that the roughening dynamics of a weakly damped interface is characterized by the scaling exponents of the Kardar-Parisi-Zhang [14] universality class. In the present work, interfacial roughening of small-amplitude capillary waves is investigated in the strong-damping regime, and the associated dynamic scaling exponents and scaling forms are derived. We show that the growth of the interfacial roughness in the strong-damping regime is qualitatively and quantitatively different from the weakly damped case. The theoretical predictions are compared against fluctuating hydrodynamics simulations of an isothermal liquid-vapor interface.

The paper is organized as follows: In the next section, the Langevin approach to capillary fluctuations of Refs. [15,16] is summarized and applied to the roughening dynamics in the strong-damping regime. Section III contains results of fluctuating hydrodynamics simulations of a single-component two-phase fluid performed with the Lattice Boltzmann method. After demonstrating that both static and dynamic equilibrium properties of capillary waves are correctly reproduced by the simulations, the nonequilibrium roughening of a fluid interface is investigated and compared to the theoretical predictions.

II. THEORY

A. General description of capillary waves

Capillary waves can be described in terms of a local height function $h(\mathbf{r}_{||})$, where $\mathbf{r}_{||}$ denotes a position in the interfacial plane (Fig. 1). The projected area of the interface is given by L^{d-1}. In the two-dimensional situation we focus upon, $r_{||} = x$, while the perpendicular coordinate is denoted by y. In the classical capillary wave theory [1–4], a capillary fluctuation is understood as a rigid shift of the "intrinsic" density profile. Thus, we can define the height function h as

$$\rho(\mathbf{r}) = \rho_{\text{int}}[y - h(\mathbf{r}_{||})], \tag{1}$$

where ρ_{int} is the intrinsic and $\rho(\mathbf{r})$ the instantaneous density profile. Since, in the present case, our treatment of a two-phase fluid is based on a Ginzburg-Landau model (see Sec. III A), we can take as the intrinsic profile the mean-field solution

$$\rho_{\text{int}}(y) = \frac{1}{2}(\rho_L + \rho_V) + \frac{1}{2}(\rho_L - \rho_V)\tanh\left(\frac{y}{w}\right), \tag{2}$$

where ρ_L and ρ_V are the liquid and vapor densities, respectively, and w is the (bare) interface width.

In our simulations, we obtain the interfacial height h by fitting ρ_{int} to the instantaneous density profile (see Fig. 1). If the interfacial height would, instead, be determined by means of a simple crossing criterion [i.e., $\rho(h) = (\rho_L + \rho_V)/2$], one would pick up local density fluctuations that are present in the interface due to its finite width. These should, however, not be interpreted as capillary waves since they are not associated with a lateral displacement of the interface profile, as expressed through Eq. (1). Local density fluctuations affect the small-scale properties of the interfacial structure and can be

*markus.gross@rub.de

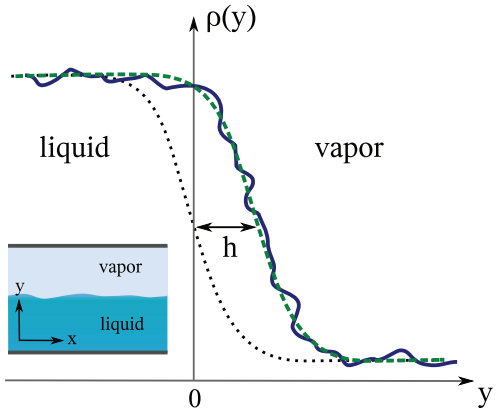

FIG. 1. (Color online) Capillary fluctuations of a planar interface. Sketch of the fluctuating density profile as a function of the lateral coordinate y. The dotted curve represents the quiescent, mean-field profile, while the dashed curve represents the fit of the mean-field profile to the instantaneous density profile (solid curve). The inset shows the simulation setup and coordinate axis.

understood in terms of interfacial density correlation functions [26–31]. In this work, however, we shall not consider them further[1] and stick to the definition of Eq. (1).

B. Langevin theory

For the description of nonequilibrium roughening, a Langevin approach to the capillary fluctuation dynamics is convenient. Such a formalism can be derived from the equations of fluctuating hydrodynamics [7,15,16], and we shall base our treatment on the Langevin theory of Refs. [15,16], which is summarized below. The general form of the Langevin equation for the height fluctuations $h_{\mathbf{k}}$ of an infinitely deep film turns out to be non-Markovian [15,16],

$$h_{\mathbf{k}}(t) = \int_{-\infty}^{t} ds\, \chi_{\mathbf{k}}(t-s) F_{\mathbf{k}}(s), \tag{3}$$

where $\chi_{\mathbf{k}}$ is a response function that, in Fourier space, is given by Refs. [15,16]

$$\chi_{\mathbf{k}}(\omega) = \frac{1}{-\mathrm{i}\omega\gamma_{\mathbf{k}}(\omega) + \sigma k^2}, \quad \text{with}$$
$$\gamma_{\mathbf{k}}(\omega) = \frac{2\omega\rho}{k\left[\mathrm{i} + \left(\frac{\mathrm{i}\omega}{\nu k^2} - 1\right)^{-1/2}\right]}, \tag{4}$$

and $F_{\mathbf{k}}$ is a random force that satisfies a fluctuation-dissipation relation

$$\langle F_{\mathbf{k}}(t) F^*_{\mathbf{k}}(0)\rangle = k_B T \gamma_{\mathbf{k}}(|t|). \tag{5}$$

Physically, the random force $F_{\mathbf{k}}$ arises from the accumulative effect of the random stress fluctuations in the bulk fluid up to a certain depth below the interface (cf. Ref. [7]). In the above equations, σ denotes the surface tension and ν the kinematic viscosity of the liquid. In this work, we adopt the Fourier-transform convention $a(\mathbf{r},t) = (2\pi)^{-d}\int d\mathbf{k} d\omega \exp(\mathrm{i}\mathbf{k}\cdot\mathbf{r} - \mathrm{i}\omega t) a_{\mathbf{k}}(\omega)$, where $\mathbf{k}$ denotes the wave vector in the $d-1$-dimensional interfacial plane (d is the spatial dimension) and ω is a frequency.

In the limit of weak damping ($\nu k^2 \to 0$) one obtains, by expanding the square root in $\gamma_{\mathbf{k}}$ of Eq. (4),

$$\gamma_{\mathbf{k},\mathrm{wd}}(\omega) = -\frac{2\rho\mathrm{i}\omega}{k} - 2\rho\mathrm{i}\sqrt{\mathrm{i}\omega\nu} + 2\rho\nu k + O(\nu^{3/2}). \tag{6}$$

Keeping in the expansion of $\gamma_{\mathbf{k},\mathrm{wd}}$ only the first and the third terms, the response function in the weak-damping limit acquires a harmonic oscillator form and is obtained from Eq. (4) as

$$\chi_{\mathbf{k},\mathrm{wd}}(\omega) = \frac{k}{2\rho}\frac{1}{-\omega^2 - \mathrm{i}\omega\nu k^2 + \frac{\sigma k^3}{2\rho}}. \tag{7}$$

In the time domain, this results in the Langevin equation

$$-\partial_t^2 h_{\mathbf{k}} + \nu k^2 \partial_t h_{\mathbf{k}} + \frac{\sigma k^3}{2\rho} h_{\mathbf{k}} = r_{\mathbf{k}}, \tag{8}$$

with $r_{\mathbf{k}}$ being a Gaussian random noise source with variance $\langle r_{\mathbf{k}}(t) r^*_{\mathbf{k}}(0)\rangle = k_B T[k\delta'(t) + \nu k^3 \delta(t)]/\rho$. The contribution $\propto \delta'(t)$ to the random force in the time domain arises from the first term in Eq. (6) and is, therefore, present even in the absence of viscosity. This is one of the most characteristic features of the present Langevin theory, which, despite the principal harmonic oscillator form of the response function, leads to quite distinct noise-driven dynamics. Equation (8) predicts capillary waves with an oscillation frequency and a damping rate given by

$$\omega_c = \left(\frac{\sigma k^3}{2\rho}\right)^{1/2}, \quad \Gamma_{\mathrm{wd}} = \nu k^2. \tag{9}$$

The slight reduction of the resonance frequency ω_c due to a finite damping has been neglected here. Note that, if the second term in Eq. (6) also is kept, the damping rate would scale $\propto k^{7/4}$ [16]. Interestingly, this type of scaling has also been derived in a few previous works based on a different theoretical approach [6,32]. In our simulations, however, we observe a behavior in agreement with Eq. (9), which can be rationalized in the context of the present Langevin theory only if the second term in Eq. (6) is neglected, as we have done above. We also remark that the relations in Eq. (9) agree well with experiments [33] and other theoretical works [34,35]. While this fact provides some sort of justification of Eq. (7), further studies would be desirable in order to clarify the relevance of the additional terms in expression (6). This, however, is out of the scope of the present work.

In the strong damping limit, one finds for $\nu k^2 \to \infty$

$$\gamma_{\mathbf{k},\mathrm{sd}}(\omega) = 4\rho\nu k - \frac{3\rho\mathrm{i}\omega}{k} + \frac{\rho\omega^2}{4k^3\nu} + O(\nu^{-2}). \tag{10}$$

Keeping only the leading term on the r.h.s. of Eq. (10), the response function follows as

$$\chi_{\mathbf{k},\mathrm{sd}}(\omega) = \frac{1}{-4\mathrm{i}\omega\rho\nu k + \sigma k^2}, \tag{11}$$

which results in the Langevin equation

$$\partial_t h_{\mathbf{k}} + \frac{\sigma k}{4\rho\nu} h_{\mathbf{k}} = \tilde{r}_{\mathbf{k}}. \tag{12}$$

[1] See, for instance, Fig. 5 in Ref. [46] for an example of a capillary wave spectrum that results when the height profile is obtained from a crossing criterion.

Here $\tilde{r}_{\mathbf{k}}$ is a Gaussian random noise source with variance $\langle \tilde{r}_{\mathbf{k}}(t)\tilde{r}^*_{\mathbf{k}}(0)\rangle = k_B T\delta(t)/4\rho\nu k$. Equation (12) implies a decay rate of

$$\Gamma_{\rm sd} = \frac{\sigma k}{4\rho\nu}. \tag{13}$$

A Langevin equation for the height fluctuations of the form of Eq. (12) has also been derived for $d > 2$ in Refs. [22,36].

Weak and strong damping regimes are separated by a critical wave number k_c. An approximate value of k_c can be obtained by noting that for small but finite damping, the capillary wave resonance in Eq. (7) appears at a frequency of $(\omega_c^2 - \Gamma_{\rm wd}^2/4)^{1/2}$, which becomes purely imaginary if $k > k_c$, where

$$k_c = \frac{2\sigma}{\rho\nu^2}. \tag{14}$$

Thus, the weak-damping regime applies to $k < k_c$ and the strong-damping regime to $k > k_c$. Clearly, the Langevin equation (12), although with slightly different numerical prefactors, could also have been directly obtained by taking the strong-damping limit of Eq. (8).

The dynamic correlation function $C(\mathbf{k},t) \equiv \langle h_{\mathbf{k}}(t)h_{-\mathbf{k}}(0)\rangle$ follows directly from Eq. (3). The static correlation function can be most easily obtained from a fluctuation-response relation as

$$C(\mathbf{k}) \equiv \langle |h_{\mathbf{k}}|^2\rangle = k_B T\chi(\mathbf{k},\omega = 0) = \frac{k_B T}{\sigma k^2}. \tag{15}$$

This classical result of capillary wave theory can also be derived from purely geometric considerations of the energy cost associated with a small-amplitude interfacial distortion [4,5]. In fact, the above result is equivalent to a harmonic approximation to the interface Hamiltonian, thus describing independent capillary waves. This is a valid approximation in the limit of small amplitudes and large wavelengths. In the presence of gravity, a finite correlation length is introduced into the static structure factor, thereby cutting off the divergence at low k [3–5]. It is useful to remark that the effective capillary wave Hamiltonian can also be obtained from a spectral analysis of a Ginzburg-Landau type of free energy functional [26,28]. Such an approach has the advantage that, in principle, the density-correlation function in the interface can be derived from first principles.

Up to numerical prefactors of the order of unity, the above expressions for the oscillation frequency and damping agree with the results of most theories of capillary wave dynamics in the literature [7,34,35,37–39]. In these theories, the liquid-vapor interface is usually taken as infinitesimally thin. The expression for ω_c in Eq. (9) has also been explicitly derived for an inviscid fluid coupled to a Ginzburg-Landau free energy functional [40]. Also, generalizations of capillary wave theory to nonzero vapor density [32,41] as well as to compressible fluids [6,39,42] have been proposed in the literature. In the case of a compressible fluid, one finds that sound waves propagating parallel to the interface give rise to an additional resonance peak in the dynamic capillary structure factor at a frequency $\omega_s \simeq c_s k$. In the present study, this frequency is typically much larger than the resonance frequency of a capillary wave and will thus be neglected.

C. Interfacial roughening

The effective *interfacial roughness* is defined as the mean square of the height amplitudes:

$$W^2(t) = \langle |h(\mathbf{r},t)|^2\rangle = \frac{1}{L^{d-1}}\sum_{\mathbf{k}}\langle |h_{\mathbf{k}}(t)|^2\rangle = \int \frac{d\mathbf{k}}{(2\pi)^{d-1}}\langle |h_{\mathbf{k}}(t)|^2\rangle, \tag{16}$$

which in equilibrium in given by Refs. [1–4,16],

$$W^2_{\rm eq} \equiv W^2(t\to\infty) \simeq \frac{k_B T}{\sigma}\times\begin{cases}\frac{1}{12}L, & \text{in 2D}\\ \log(L/l_0), & \text{in 3D}\end{cases}, \tag{17}$$

where l_0 is the minimal length scale available in the system. In the 2D case, the sum has been computed using the relation $\sum_{n=1}^{\infty} 1/n^2 = \pi^2/6$, whereas in the 3D case, it has been approximated by an integral. It is important to realize that, both in two and three dimensions, the interfacial roughness is diverging with the system size, although this divergence is very weak in three dimensions. The time evolution of the interface height under the action of the random force can be computed directly from the Langevin equation (3), explicitly assuming that $F_{\mathbf{k}}(s) = 0$ for $s < 0$, since we are interested in the growth from a quiescent state at $t = 0$. Note also that, due to causality, $\chi_{\mathbf{k}}(t) = 0$ for $t < 0$.

Roughening in the *weak-damping limit* has already been discussed in Refs. [15,16], of which the essential results shall be summarized first. Neglecting the effect of viscosity, which is sufficient to determine the leading order behavior, the response function in the time domain follows from Eq. (7) as Refs. [15,16]

$$\chi_{\mathbf{k},\rm wd}(t) = \frac{k}{2\rho\omega_c}\sin(\omega_c t)\theta(t), \tag{18}$$

from which the equal-time height correlation function can be obtained as

$$\begin{aligned}&\langle |h_{\mathbf{k},\rm wd}(t)|^2\rangle\\ &= \int_0^t ds\int_0^t ds'\chi_{\mathbf{k},\rm wd}(t-s)\chi_{\mathbf{k},\rm wd}(t-s')\langle F_{\mathbf{k}}(s)F^*_{\mathbf{k}}(s')\rangle\\ &= \frac{2k_B T}{\sigma k^2}\sin^2(\omega_c t).\end{aligned} \tag{19}$$

Due to the neglect of viscosity, the correlation function describes infinitely oscillating capillary waves. It is useful to note that, at early times ($t \ll 1/w_c$), $\langle |h_{\mathbf{k}}(t)|^2\rangle$ grows $\propto t^2$ [Fig. 2(a)]. The time-dependent interfacial roughness, Eq. (16), follows in the 2D case from Eq. (19) as Ref. [16]

$$\begin{aligned}W^2_{\rm wd}(t) &= \frac{k_B T}{\pi\sigma}\int_{k_{\rm min}}^{k_{\rm max}} dk\frac{\sin^2(\omega_c t)}{k^2}\\ &= t^{2/3}\frac{2k_B T}{3\pi(2\rho\sigma^2)^{1/3}}\int_{\omega_{c,\rm min}t}^{\omega_{c,\rm max}t} dx\frac{\sin^2 x}{x^{5/3}},\end{aligned} \tag{20}$$

where $k_{\rm min}$ and $k_{\rm max}$ are the smallest and largest possible wave numbers in the system and $\omega_{c,\rm min,max}$ are the corresponding capillary wave frequencies. In the last step, the substitution $x = \omega_c t$ has been made to exhibit the leading time dependence. In the range where $\omega^{-1}_{c,\rm max} \lesssim t \lesssim \omega^{-1}_{c,\rm min}$, the value of the integral is roughly constant and, consequently, $W_{\rm wd}(t)$ grows

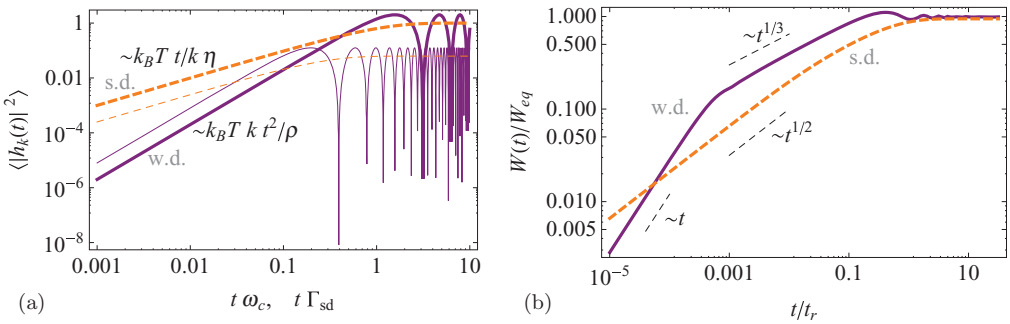

FIG. 2. (Color online) Theoretical predictions of the growth of (a) the height amplitude $\langle|h_{\mathbf{k}}(t)|^2\rangle$ [Eqs. (19) and (24)] and (b) the interfacial roughness $W(t)$ [Eqs. (20) and (25)] in the 2D case. The solid and dashed curves correspond to the weak-damping ("w.d.") and strong-damping ("s.d.") regime, respectively. (a) The thin curves additionally show the growth of a large wave number mode ($k' > k$), whose time and length is scaled with the same factors as the small wave number mode (thick curves) for better comparison. Time is scaled by the resonance frequency ω_c [Eq. (9)] or relaxation rate Γ_{sd} [Eq. (13)], depending on the regime. (b) Time is scaled by the corresponding roughening times, Eqs. (21) and (27).

like $t^{1/3}$. At early times, $W_{wd}(t)$ grows linearly in time [Fig. 2(b)], reflecting the quadratic growth of the height-correlation function [Eq. (19)]. Note that the extent of the early-time regime decreases relative to the late-time regime when the size L of the interface is increased. In the 3D case, we have logarithmic growth, $W^2_{wd}(t) \propto \log t$ [16]. The time after which the roughness reaches its equilibrium value can be estimated as a quarter of a period of the capillary wave with the largest wavelength,

$$t_{r,wd} \simeq \sqrt{L^3\rho/(16\pi\sigma)}. \tag{21}$$

In the *strong-damping limit*, the Fourier transform of Eq. (11) yields

$$\chi_{\mathbf{k},sd}(t) = \frac{1}{4\eta k}\exp\left(-\frac{\sigma k}{4\eta}t\right)\theta(t). \tag{22}$$

From the expression for the correlations of the random force in this limit,

$$\langle F_{\mathbf{k}}(t)F^*_{\mathbf{k}}(0)\rangle = 4\rho\nu k k_B T\delta(|t|), \tag{23}$$

the equal-time height-correlation function results as

$$\langle|h_{\mathbf{k},sd}(t)|^2\rangle = \frac{k_B T}{\sigma k^2}\left[1-\exp\left(-\frac{\sigma k}{2\eta}t\right)\right]. \tag{24}$$

Note that $\langle|h_{\mathbf{k},sd}(t)|^2$ approaches the expression for the static spectrum, Eq. (15), in the long-time limit. According to Eq. (24), the height variance grows $\propto t$ at small times until, after roughly a time scale of the order of the capillary time ($\sim\eta/\sigma k$), it reaches equilibrium [Fig. 2(a)]. In the 2D case, the roughness follows from Eq. (24) as

$$\begin{aligned} W^2_{sd}(t) &= t\frac{k_B T}{4\pi\eta}\int_{ak_{min}t}^{ak_{max}t} dx\,\frac{1-\exp(-x)}{x^2} \\ &= t\frac{k_B T}{4\pi\eta}[\Gamma(-1,x) - x^{-1}]|_{x=ak_{min}t}^{x=ak_{max}t}, \end{aligned} \tag{25}$$

where $a \equiv \sigma/2\eta$ and $\Gamma(n,x)$ is the incomplete γ function. As long as $(ak_{max})^{-1} \lesssim t \lesssim (ak_{min})^{-1}$, the leading time dependence is unaffected by the expression in the square brackets, and the roughness thus grows as $W_{sd}(t) \propto t^{1/2}$ until equilibrium is reached. At early times, $W_{sd}(t)$ is expected to grow linearly, which is related to higher-order frequency terms that are neglected in Eq. (11) (see Appendix for further discussion). In the 3D case, we find

$$W^2_{sd}(t) = \frac{k_B T}{4\pi\sigma}[-\mathrm{Ei}(-x) + \log x]|_{x=ak_{min}t}^{x=ak_{max}t}, \tag{26}$$

where Ei denotes the exponential integral function. In the range $(ak_{max})^{-1} \lesssim t \lesssim (ak_{min})^{-1}$, $W^2_{sd}(t) \propto \log t$, which is preceded by a linear growth at earlier times. The roughening time in the strong-damping regime can be approximated as the inverse of the overdamped relaxation rate of Eq. (13) evaluated for the largest wave number,

$$t_{r,sd} \simeq \eta L/\pi\sigma. \tag{27}$$

Note that, at late times, the normalization of the above $W^2_{sd}(t)$ is slightly different from the exact equilibrium result based on the sum over the discrete wave modes, Eq. (17).

The origin of the different scaling behavior for the roughness in Eqs. (20) and (25) lies in the different growth speeds of the individual height amplitudes $\langle|h_{\mathbf{k}}(t)|^2\rangle$ in dependence of the wave number [Fig. 2(a)]. In the strong-damping case, the growth rate scales $\propto 1/k$ at early times; i.e., the mode with the smallest wave number grows fastest, and the roughness essentially reflects the growth of this mode. In contrast, in the weak-damping case, modes of larger k grow faster, and the early linear growth of W is essentially due to the largest k-mode available in the system. However, since large-k modes also reach equilibrium earlier [from Eq. (19), their roughening time is $\propto k^{-3/2}$], there appears a $t^{1/3}$ regime in the weak-damping case where the growth of W is due to a "saturation" effect of subsequently smaller k modes, until, finally, also the mode with the smallest k has reached equilibrium.

Neglecting the very early growth, it is seen that, in the 2D case, the roughness $W(t)$ obeys a scaling relation

$$\begin{aligned} &W(t) = L^\alpha w(t/L^z), \quad \text{with} \\ &\alpha = 1/2, \begin{cases} z = 3/2 \ \text{(weak damping)} \\ z = 1 \ \text{(strong damping)} \end{cases}. \end{aligned} \tag{28}$$

The scaling index α is an equilibrium property of the roughness [Eq. (17)] and is independent of the damping regime. The scaling function $w(x)$ reaches a constant for $x \to \infty$ and

behaves as

$$w(x) \sim x^{\alpha/z} \tag{29}$$

for small x. As noted in Refs. [16,25], in the weak-damping limit, the scaling properties of W fall into the Kardar-Parisi-Zhang universality class of surface growth [14].[2] However, as shown here, the Langevin theory predicts a different dynamical scaling index z for strong damping.[3] In three dimensions, the roughening proceeds logarithmically both in the weak and strong damping regime and cannot be characterized by scaling exponents.

III. SIMULATIONS

A. Model and setup

Our simulations are based on the fluctuating Lattice Boltzmann (LB) method [43–45], which was extended to nonideal fluids in Ref. [46] (see also Refs. [47,48] for further discussions). The underlying deterministic LB model, on which our fluctuating LB approach is based, was introduced in Refs. [49,50]. For general information on the LB method we refer to the numerous reviews available [51–53]. For the present purposes, it suffices to note that this method solves the equations of fluctuating hydrodynamics of an isothermal nonideal fluid [40,54–58]. The fluctuating hydrodynamic equations describe the evolution of a fluctuating density and velocity field $\rho(\mathbf{r})$, $\mathbf{u}(\mathbf{r})$ and consist of a continuity equation,

$$\partial_t \rho = -\nabla \cdot (\rho \mathbf{u}) \tag{30}$$

and a momentum conservation equation,

$$\partial_t(\rho \mathbf{u}) + \nabla \cdot (\rho \mathbf{u}\mathbf{u}) = -\nabla \cdot \mathbf{P} + \nabla \cdot \Pi + \nabla \cdot \mathbf{R}. \tag{31}$$

Here Π is the viscous stress tensor

$$\Pi_{\alpha\beta} = \eta\left(\partial_\alpha u_\beta + \partial_\beta u_\alpha - \frac{2}{d}\delta_{\alpha\beta}\partial_\gamma u_\gamma\right) + \zeta\,\partial_\gamma u_\gamma \delta_{\alpha\beta}, \tag{32}$$

$\mathbf{R}$ the random stress tensor with Gaussian correlations characterized by

$$\begin{aligned}\langle R_{\alpha\beta}(\mathbf{r},t)R_{\gamma\delta}(\mathbf{r}',t')\rangle &= 2k_BT\left[\eta\left(\delta_{\alpha\gamma}\delta_{\beta\delta} + \delta_{\alpha\delta}\delta_{\beta\gamma} - \frac{2}{d}\delta_{\alpha\beta}\delta_{\gamma\delta}\right) + \zeta\,\delta_{\alpha\beta}\delta_{\gamma\delta}\right] \\ &\quad \times \delta(\mathbf{r}-\mathbf{r}')\delta(t-t'),\end{aligned} \tag{33}$$

and η and ζ the shear and bulk viscosity. As a peculiarity of the LB method, η and ζ are in general proportional to the density, but can otherwise be freely tuned. For generality, we have kept the spatial dimensionality d here. The physics of a nonideal fluid enters the model via the pressure tensor [3,40,58]

$$P_{\alpha\beta} = \left(p_0 - \kappa\rho\nabla^2\rho - \frac{\kappa}{2}|\nabla\rho|^2\right)\delta_{\alpha\beta} + \kappa(\partial_\alpha\rho)(\partial_\beta\rho), \tag{34}$$

where p_0 is a given equation of state (bulk pressure) and κ a square-gradient parameter. In fact, the above form of the pressure tensor $\mathbf{P}$ can be derived from a Ginzburg-Landau free energy functional

$$\mathcal{F}[\rho] = \int d\mathbf{r}\left[\frac{\kappa}{2}|\nabla\rho|^2 + f_0(\rho)\right], \tag{35}$$

since

$$\nabla \cdot \mathbf{P} = \rho\nabla\frac{\delta\mathcal{F}}{\delta\rho}. \tag{36}$$

Here f_0 is a Landau free energy density, fulfilling

$$p_0 = \rho\partial_\rho f_0 - f_0. \tag{37}$$

We take f_0 to be of a simple double-well form with minima at the equilibrium densities ρ_V, ρ_L [4,59,60],

$$f_0(\rho) = \beta(\rho-\rho_V)^2(\rho-\rho_L)^2. \tag{38}$$

Note that for a symmetric Ginzburg-Landau free energy functional [as in Eq. (35)] the bending rigidity, and with it the Tolman correction, which describes the dependence of the surface tension on curvature [61], vanishes [62]. In the absence of flow and thermal noise, the equilibrium solution of Eqs. (30), (31), and (38) fulfils $\nabla \cdot \mathbf{P} = 0$ and describes, in the simplest case, a liquid and a vapor phase separated by a diffuse interface. The profile is given by Eq. (2), with a width of

$$w = \frac{2}{\rho_L - \rho_V}\sqrt{\frac{2\kappa}{\beta}}. \tag{39}$$

Thermal noise, which is imparted by the random stress tensor $\mathbf{R}$ throughout the fluid, leads to the excitation of capillary waves on the interface [7,15,16,40]. Only a small number of previous simulation studies of fluctuating interfaces in continuum hydrodynamic models exist, of which the ones most relevant for the present context are based on lattice gas automata [15,16,25] (see also Ref. [63]). Recently, also a fluctuating LB scheme for the Kardar-Parisi-Zhang equation has been introduced [64].

All our simulations are performed in two dimensions. We place a liquid stripe of size $L_X \times H$ in a rectangular box of size $L_X \times L_Y$, where L_Y is typically $\sim 2H \simeq 128$ lattice units (l.u.) and L_X varies between 128 and 512 l.u. The box is periodic in x-direction and covered by substrates at the boundaries in y-direction (see Fig. 1). The ratio of the equilibrium roughness to the film thickness is less than $O(10^{-2})$. We expect our results to approximate the limit of infinitely deep films and have checked in a few cases, by increasing H and L_Y, that our results are insensitive to the film height. Static properties of capillary fluctuations turn out to be quite insensitive to the specific simulation parameters in the present model. In contrast, regarding dynamics, satisfactory agreement between theory and simulation results was found to require quite large liquid-vapor density ratios (around $\rho_L/\rho_V = 100$) and intrinsic interface widths not larger than 5 l.u.

B. Equilibrium properties

Before we turn to interfacial roughening, a number of basic equilibrium properties of capillary waves are discussed. This not only serves as a validation of the simulation method, but is also important since, owing to the fluctuation-dissipation relation, equilibrium dynamics and nonequilibrium roughening

[2] As noted previously [16], this might be by coincidence, though, since the growth mechanism described by the Kardar-Parisi-Zhang equation is different from the roughening of a fluid interface.

[3] Interestingly, in the strong-damping case, the dynamic exponents given in Eq. (28) can also be derived from the renormalization group study of Ref. [22], although the results obtained there are formally valid only for $d > 2$.

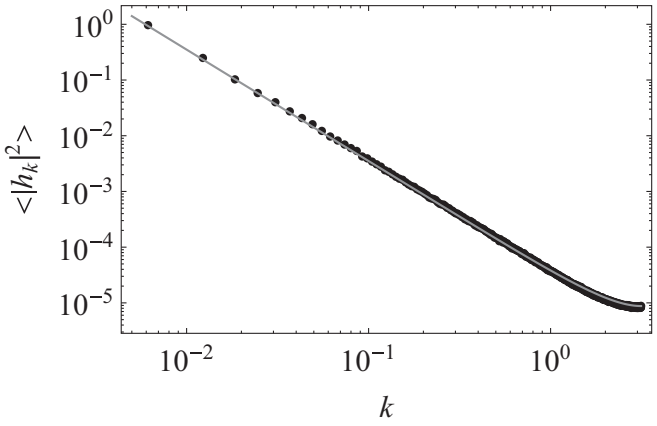

FIG. 3. Equal-time spectrum of interfacial height fluctuations on a planar one-dimensional interface obtained from LB simulations (filled circles), compared to the theoretical capillary structure factor [solid line, Eq. (15)]. k denotes the wave number in the plane of the interface. Simulation parameters: $L = 1024$, $\rho_L = 1.0$, $\rho_V = 0.5$, $\beta = 0.11$, $\kappa = 0.08$, $k_BT = 10^{-7}$, $\tau = 1.0$, surface tension $\sigma \simeq 2.7 \times 10^{-3}$, interface width approximately 5 l.u.

are governed by the same kinetic coefficients. In Fig. 3, the static (equal-time) capillary wave correlation function $\langle h_{\mathbf{k}} h_{-\mathbf{k}} \rangle$ obtained from our simulations is shown (see also Ref. [47]). The real-space height profile $h(\mathbf{r})$ is extracted by fitting the mean-field profile, Eq. (2), at each point $\mathbf{r}$ to the instantaneous density profile obtained from the simulation. The spectrum is computed, after neglecting the initial roughening period, by averaging over 2000 snapshots in a simulation running for 10^6 time steps, which is around one order of magnitude larger than the largest possible relaxation time of a capillary fluctuation in the system, as inferred from Eq. (21) or (27) (both of which give similar estimates). Perfect agreement between the simulation results and the theoretical capillary structure factor, Eq. (15), is found for practically all wave numbers. Note that, on a lattice, k^2 in Eq. (15) has to be replaced by (the negative of) the Fourier transform of the proper one-dimensional discrete Laplacian, $2 - 2\cos k$. The discrete nature of the Laplacian is the reason for the upturn of the structure factor at large wave numbers in Fig. 3. The difference between the continuum and lattice Laplacian is significant only for large wave numbers ($k \gtrsim 1$).

Figure 4(a) shows simulation results on the capillary wave correlation function $C(\mathbf{k},t) \equiv \langle h_{\mathbf{k}}(t) h_{-\mathbf{k}} \rangle$ in the weak-damping regime (see caption to Fig. 4 for simulation parameters), where an oscillatory decay,

$$C(\mathbf{k},t) = \langle |h_{\mathbf{k}}|^2 \rangle \exp(-\Gamma_{\mathrm{wd}}|t|) \cos(\omega_c t), \tag{40}$$

with a frequency and damping rate given by Eq. (9), is predicted by the theory. Since the damping rate increases quadratically with k, waves with larger wave numbers are seen to oscillate for not more than a single period until they become practically indistinguishable from the background noise. Figure 4(b) shows the oscillation frequency and damping rate extracted by fitting expression (40) to the simulation data. The dashed lines represent $\sqrt{2}\omega_c$ and $2\Gamma_{\mathrm{wd}}$, where the prefactors have been included here in order to conform with the expressions of standard capillary wave theories. It is seen that, after the correction for numerical prefactors, both quantities compare well to the theoretical predictions up to a wave number of $k \simeq 0.7$. Deviations at higher wave numbers are partly attributed to the fact that the damping is so strong that it is hard to unambiguously extract both the frequency and damping rate from the data. Additionally, the hydrodynamic regime, where the transport coefficients are constants, generally breaks down in LB at large wave numbers [65,66].

In the case of overdamped dynamics, capillary waves decay purely exponentially:

$$C(\mathbf{k},t) = \langle |h_{\mathbf{k}}|^2 \rangle \exp(-\Gamma_{\mathrm{sd}}|t|), \tag{41}$$

which is clearly seen in the logarithmic plot in Fig. 5(a). Figure 5(b) shows the relaxation rate, obtained by fitting Eq. (41) to the data. After correcting for a numerical prefactor of 2, the theoretical prediction is well reproduced up to a wave number of $k \simeq 0.5$. Similarly to the previous case, a possible reason for the noticeable deviations at larger wave numbers might be that the viscosity becomes wave number dependent for larger k. It should also be noted that the above results are obtained in the limit of small vapor density ($\rho_V = 0.01\rho_L$). For larger vapor

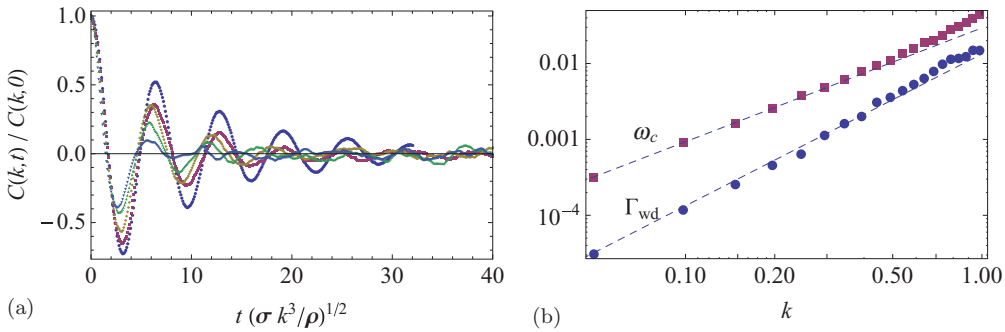

FIG. 4. (Color online) Capillary waves on a planar interface in the weak-damping regime. (a) The correlation function $C(k,t)$ obtained from simulations (normalized to its equilibrium value) is shown for different wave numbers $k = 2\pi n/L$, where $n = 1$ (●), 3 (■), 5 (♦), 7 (▲), 9 (▼). The time axis is scaled by the theoretical resonance frequency w_c, Eq. (9). (b) The data for the capillary wave resonance frequency $\omega_c(k)$ (■) and damping rate $\Gamma(k)$ (●) are shown. The dashed lines represent the theoretical predictions of Eq. (9), $\sqrt{2}\omega_c$ and $2\Gamma_{\mathrm{wd}}$, corrected by numerical prefactors. Simulation parameters: $L = 128$, $\rho_L = 1.0$, $\rho_V = 0.01$, $\beta = 0.0024$, $\kappa = 0.006$, $\nu = 0.00667$, $k_BT = 10^{-8}$, surface tension $\sigma = 8.7 \times 10^{-4}$, interface width $\simeq$5 l.u.

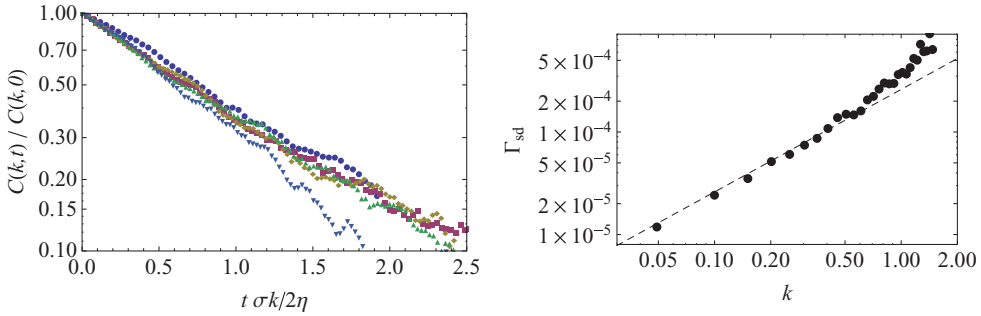

FIG. 5. (Color online) Capillary waves on a planar interface in the strong-damping regime. (a) The correlation function $C(k,t)$ obtained from simulations (normalized to its equilibrium value) is shown for different wave numbers $k = 2\pi n/L$, where $n = 1$ (●), 3 (■), 5 (♦), 7 (▲), 9 (▼). The time axis is scaled by the theoretical relaxation rate, Eq. (13). (b) The data for the damping rate in the overdamped regime are shown. The dashed line represents the theoretical prediction of Eq. (13), $2\Gamma_{\rm sd}$, corrected by a numerical prefactor. Simulation parameters: $L = 128$, $\rho_L = 1.0$, $\rho_V = 0.01$, $\beta = 0.00024$, $\kappa = 0.0006$, $\nu = 0.167$, $k_BT = 10^{-9}$, surface tension $\sigma = 8.7 \times 10^{-5}$, interface width $\simeq$5 l.u.

densities, the agreement between simulation and theoretical predictions is found to become worse, even when comparing to theoretical expressions that take into account a finite vapor density [32,41]. We also observe that the discrepancies grow when the interfacial width is further increased. The origin of this behavior is presently unknown. Thus, in the future, a closer theoretical investigation of capillary wave dynamics in diffuse interface models would be interesting, taking also into account effects of a finite vapor density, which seems to have not been done in a sufficiently general way up to now [40,67].

Of course, since the above results pertain to the linear-response regime (where the fluctuation amplitudes are small by definition), they could have equivalently been obtained from a study of individual capillary waves in a simulation without thermal noise (Onsager regression hypothesis). Previous LB studies of capillary wave dynamics made use of this equivalence and obtained capillary wave dispersion relations similar to the present work [49,68,69]. In contrast to the equilibrium relaxation dynamics, however, the interfacial roughening phenomenon studied in the next section is a genuinely fluctuation induced effect.

C. Interfacial roughening

Figures 6 and 7 show simulation results for the time evolution of the interfacial roughness in the weak- and strong-damping regimes. It has been made sure, by choosing simulation parameters appropriately (see Table I), that all wave modes existing on the interface exclusively fall in either one of the considered regimes. In all cases, the interfacial width is 5 l.u. and the density ratio of $\rho_L/\rho_V = 100$ is used in order to approximate the case of zero vapor density (upon which the theoretical derivation is based) as closely as possible. To ensure sufficient statistical accuracy, the roughness is computed by averaging over 10–30 independent simulations. Since it was seen in Fig. 3 that the static capillary correlations are correctly reproduced, it is clear that the equilibrium interfacial roughness [Eq. (17)], which is essentially determined by the integrated structure factor, also agrees with the theoretical predictions. Therefore, $W_{\rm eq}$ is not discussed separately here, but instead, we turn directly to the time evolution of the roughness.

In Fig. 6(a), the time-dependent interfacial roughness $W(t)$ in the weak-damping case is plotted, with each curve corresponding to a simulation performed for different values of surface tension, viscosity, and fluctuation temperature, keeping the system size fixed. Data collapse is achieved by rescaling time by the roughening time $t_{r,\rm wd}$, Eq. (21), and the roughness by its expected equilibrium value $W_{\rm eq}$, Eq. (17). We see that the overall trend of the data is correctly captured by the theory (dashed curve), with a linear growth at early times and a $t^{1/3}$ growth at late times, until at around a time $t_{r,\rm wd}$ the roughness

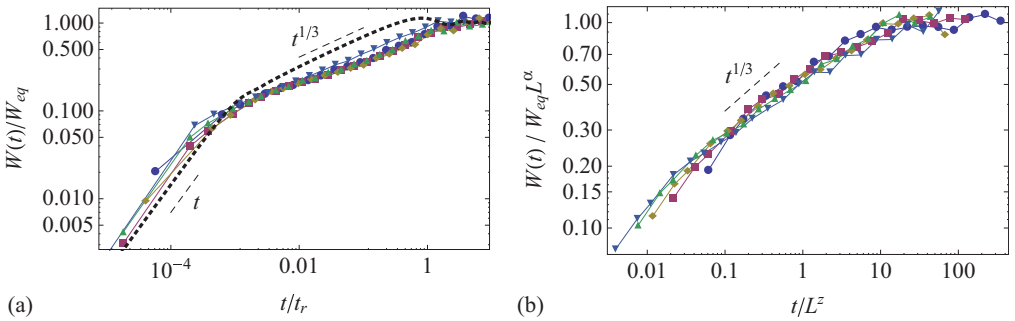

FIG. 6. (Color online) Time evolution of the interfacial roughness W in the *weak-damping* regime. (a) Data obtained for different values of surface tension, viscosity, and fluctuation temperature (see Table I) and a fixed system size of $L = 512$ are plotted. The thick dotted curve represents the theoretical prediction, Eq. (20). Time is scaled by the roughening time t_r [Eq. (21)] and the roughness is scaled by its equilibrium value $W_{\rm eq}$. (b) Simulation parameters are fixed at $\rho_L = 1.0$, $\rho_V = 0.01$, $\sigma = 8.7 \times 10^{-4}$, $\nu = 6.7 \times 10^{-3}$, $k_BT = 10^{-8}$, and the system size is varied as $L = 32$ (●), 64 (■), 96 (♦), 128 (▲), 200 (▼). The values of the scaling exponents are $\alpha = 1/2$ and $z = 3/2$.

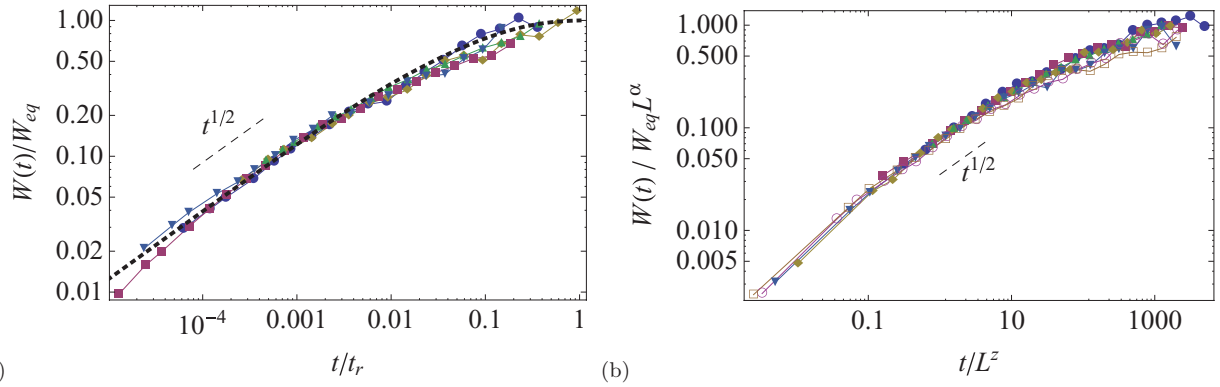

FIG. 7. (Color online) Time evolution of the interfacial roughness W in the *strong-damping* regime. (a) Data obtained for different values of surface tension, viscosity, and fluctuation temperature (see Table I) and a fixed system size of $L = 128$ are plotted. The thick dotted line represents the theoretical prediction, Eq. (25). Time is scaled by the roughening time t_r [Eq. (27)] and the roughness is scaled by its equilibrium value $W_{\rm eq}$. (b) Simulation parameters are fixed at $\rho_L = 1.0$, $\rho_V = 0.01$, $\sigma = 3.6 \times 10^{-5}$, $\nu = 0.17$, $k_BT = 10^{-9}$, and the system size is varied as $L = 32$ (●), 64 (■), 96 (♦), 128 (▲), 200 (▼), 300 (○), 400 (□). The values of the scaling exponents are $\alpha = 1/2$ and $z = 1$.

attains its equilibrium value. In the crossover region between the two growth regimes, however, the roughness is found to grow significantly slower than predicted by the theory. In fact, the data seem to be more consistent with a $t^{1/4}$ behavior at intermediate times. This effect is more pronounced for small system sizes and also found to slightly depend on the chosen simulation parameters.

In Fig. 6(b) the roughness is shown for different system sizes between $L = 32$ and 200 l.u., keeping all other system parameters the same. By scaling time with L^z ($z = 3/2$) and $W(t)$ with L^{α} ($\alpha = 1/2$), it is seen that all data points approximately collapse onto a single master curve with a logarithmic slope of $\alpha/z = 1/3$, as expected from the scaling form Eq. (28). However, we remark that a satisfactory scaling collapse could also be achieved with an index of $z = 2$ (or any other value between 3/2 and 2), corresponding to a growth behavior $W \sim t^{1/4}$ in Fig. 6(a). While the reason for these discrepancies between simulation and theory is unclear at present, we note that these deviations cannot be explained by the influence of a finite viscosity, since in that case one would expect to approach a $t^{1/2}$ power law with increasing viscosity and, thus, find an even larger exponent than 1/3 (cf. Fig. 8). Also, the effect seems not to be related to the density ratio between liquid and vapor, as we have obtained essentially the same results for different values of ρ_L/ρ_V ranging between 0.5 and 0.001.

TABLE I. Simulation parameters (surface tension σ, kinematic shear viscosity ν, and fluctuation temperature k_BT) used in Figs. 6(a) and 7(a). In both cases, $\rho_L = 1.0$ and $\rho_V = 0.01$. All parameters are given in l.u.

	Weak damping [Fig. 6(a)]			Strong damping [Fig. 7(a)]		
	σ	ν	k_BT	σ	ν	k_BT
●	8.7×10^{-3}	0.017	10^{-8}	8.7×10^{-5}	0.17	10^{-9}
■	8.7×10^{-4}	3.3×10^{-3}	10^{-9}	3.6×10^{-6}	0.033	10^{-10}
♦	4.3×10^{-3}	6.7×10^{-3}	10^{-8}	7.2×10^{-4}	0.33	10^{-10}
▲	8.7×10^{-4}	6.7×10^{-3}	10^{-8}	3.6×10^{-5}	0.17	10^{-9}
▼	1.4×10^{-5}	5.0×10^{-3}	10^{-10}	3.6×10^{-6}	0.17	10^{-10}

Figure 7 shows the time evolution of the interfacial roughness in the strong-damping regime. In Fig. 7(a), the data are obtained from simulations of varying fluid parameters but identical system size, while in Fig. 7(b) only the system size is varied. Good agreement with the theoretical predictions [Eq. (25)] over approximately three orders of magnitude is found. In particular, the data agree well with the derived scaling function [dashed curve in Fig. 7(a)] and the approximate power-law growth of the roughness $\propto t^{1/2}$ is recovered. At early times, some deviations from a pure power-law behavior are visible, which can be attributed to the neglect of terms beyond linear order in the frequency dependence of the response function [see Eq. (11)]. This point is further discussed in the Appendix. In contrast to the weak-damping case, no rescaling of time in the plot of the theoretical $W(t)$ is found to be necessary. The scaling collapse of the data in Fig. 7(b)

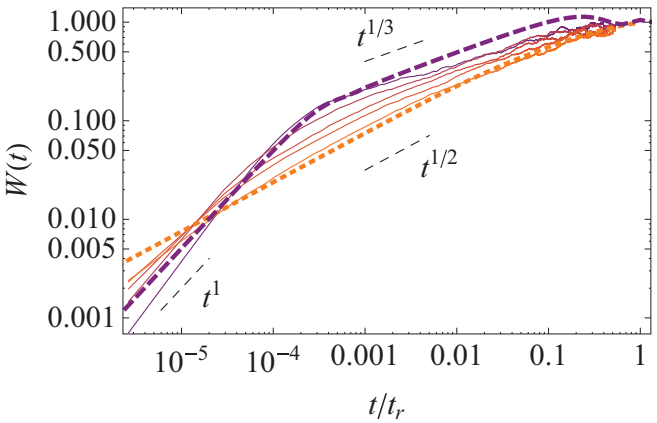

FIG. 8. (Color online) Time evolution of the roughness in the crossover region between weak and strong damping. The dashed and dotted curves represent the expressions for W in the weak- and strong-damping limit, Eqs. (20) and (25), respectively. Simulation data are shown as thin curves for visibility, corresponding to viscosities of $\nu = 0.0033, 0.0167, 0.04, 0.067, 0.133$ l.u. The other simulation parameters are fixed at $\rho_L = 1.0$, $\rho_V = 0.01$, $\sigma = 1.4 \times 10^{-5}$, $k_BT = 10^{-10}$, $L = 128$. Time is rescaled by the roughening time corresponding to the strong-damping limit, Eq. (27).

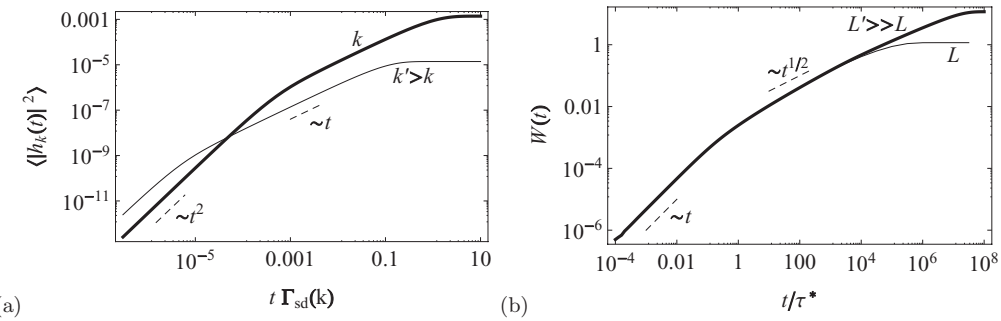

FIG. 9. Early-time dynamics in the overdamped regime. (a) Equal-time height-correlation function, taking into account the leading-order frequency dependence [Eq. (A4)], for two different wave numbers k and $k' > k$. Time is scaled by the damping rate [Eq. (13)] corresponding to the wave number k. (b) Time evolution of the roughness based on expression (A4), for two different system sizes, L and $L' = 100L$. Time is scaled by the crossover time $\tau^* = 1/k_{\max}^2\nu$ between early- and late-time behavior.

is achieved with a dynamical index $z = 1$, confirming that the roughening dynamics in the overdamped case belongs to a different universality class than in the weak-damping case.

Finally, we investigate in Fig. 8 the roughness in the crossover region from weak to strong damping. The simulation data (thin solid lines) in Fig. 8 have been obtained by successively increasing the viscosity from small to large values, keeping all other system parameters fixed. Due to the non-Markovian nature of the interface dynamics in the crossover regime, it is difficult to obtain an analytic expression for $W(t)$ in this case. We observe that the simulation data smoothly interpolate between the overdamped (thick dotted line) and underdamped (thick dashed line) limits. Similarly to Fig. 6(a), deviations between simulations and theory are noticeable at intermediate times in the limit of weak damping [they appear to be more pronounced here due to the smaller system size than in Fig. 6(a)].

IV. SUMMARY

We have investigated in this work the dynamics of capillary waves and the nonequilibrium roughening of a liquid-vapor interface based on an effective Langevin description and by means of fluctuating hydrodynamics simulations using the Lattice Boltzmann method. Although roughening is a well-known mechanism of film growth, its counterpart in thermally excited fluid interfaces seems to have been only rarely studied [15,16,22,25]. As a central result, we showed that the nonequilibrium growth of the roughness proceeds by different dynamical scaling laws, depending on whether the system is either weakly or strongly damped [see Eq. (28)]. In the weak-damping case, we find basic agreement between our Lattice Boltzmann simulations and previous works [15,16,25], which observed scaling exponents characteristic for the Kardar-Parisi-Zhang universality class ($\alpha = 1/2$, $z = 3/2$). We remark, however, that an dynamic exponent of $z = 2$ can also not be fully excluded based on the present data. In the strong damping case, the roughening is governed by a dynamic scaling exponent $z = 1$, which is characteristic for an overdamped harmonic oscillator driven by white noise. The scaling exponent α, related to the size dependence of the equilibrium roughness, is found to be equal to $1/2$, in agreement with the theory.

ACKNOWLEDGMENTS

We would like to thank A. J. Wagner for useful discussions. Funding from the industrial sponsors of ICAMS, the state of North-Rhine Westphalia, and the European Commission in the framework of the European Regional Development Fund (ERDF) is gratefully acknowledged.

APPENDIX: EARLY-TIME BEHAVIOR

Relation (11) and thus Eq. (25) for the roughness in the case of strong damping becomes exact in the limit of infinite viscosity. For large but finite viscosity, Eq. (25) describes the growth only at sufficiently late times, since, by keeping only the leading term in the expansion of Eq. (10), the high-frequency aspects of the dynamics have been neglected. In the case of weak damping, we expect the early-time properties to be correctly described by Eq. (20), since the leading term in the expansion of Eq. (6) is already the dominant one for large frequencies. Some insights into the early-time growth of a strongly damped interface can be gained by retaining the leading frequency-dependent term in $\gamma_{\rm sd}$. This results in a harmonic-oscillator form of the response function

$$\chi_{\mathbf{k},\rm sd}(\omega) = \frac{k}{3\rho}\,\frac{1}{-\omega^2 - \frac{4}{3}\nu k^2 \mathrm{i}\omega + \sigma k^3/3\rho}, \qquad \text{(A1)}$$

which becomes in real space

$$\chi_{\mathbf{k},\rm sd}(t) = \frac{k}{3\rho D}\exp\left(-\frac{2}{3}\nu k^2 t\right) 2\sinh\left(\frac{1}{2}Dt\right), \qquad \text{(A2)}$$

with $D \equiv \sqrt{16\nu^2k^4/9 - 4\sigma k^3/3\rho}$. The correlations of the random force acquire now, in addition to expression (23), a contribution proportional to the derivative of a δ function,

$$\langle F_{\mathbf{k}}(t)F^*_{\mathbf{k}}(0)\rangle = k_B T\left[4\rho\nu k\delta(t) + \frac{3\rho}{k}\delta'(t)\right]. \qquad \text{(A3)}$$

When computing the height correlation function, this term is treated as in the weak-damping case [16]. In this way, we find

$$\langle|h_{\mathbf{k}}(t)|^2\rangle = \frac{k_B T}{2\sigma k^2}\left[1 - \exp\left(-\frac{4}{3}k^2\nu t\right)\right.$$
$$\left.\times\left(\cosh Dt - \frac{4\nu k^2}{3D}\sinh Dt\right)\right]. \qquad \text{(A4)}$$

The correlation function (A4) is plotted in Fig. 9(a) for two different wave numbers. The early-time growth of the height-correlation function can be more directly assessed by neglecting the "mass term" $\sigma k^3/3\rho$ in the response function (A1), yielding

$$\langle |h_{\mathbf{k}}(t)|^2 \rangle \simeq \frac{k_B T}{32 k^3 \nu^2 \rho} \left[8k^2 \nu t + 3 \exp\left(-\frac{8}{3} k^2 \nu t \right) - 3 \right]. \tag{A5}$$

Thus, for small times, the height correlation function grows $\propto kt^2$, until for $t \gtrsim (\nu k^2)^{-1}$, crossover to linear growth, characteristic of the overdamped case in the infinite-viscosity limit (Brownian dynamics), occurs. As an artifact of neglecting the surface tension, the system roughens for an infinite time. Note that since the frequency expansion of γ_{sd} has been truncated after the linear order term [Eq. (10)], a different growth behavior might result at still earlier times.

Figure 9(b) shows the time-dependent roughness obtained by integrating Eq. (A4) over all wave numbers of a finite system. The early-time growth of $\langle |h_{\mathbf{k}}(t)|^2 \rangle$ is directly reflected in the linear growth of $W(t)$, while the $t^{1/2}$ growth characteristic for an overdamped system sets in after a crossover time τ^*. We find that $\tau^* \simeq (k_{\mathrm{max}}^2 \nu)^{-1}$ is determined only by the viscosity and the largest wave number of the system (here $k_{\mathrm{max}} = \pi/l_0$), but is independent of the system size. Thus, for $\nu \to \infty$ or $L \to \infty$, the growth of the roughness will be completely dominated by the late-time behavior, where the scaling expressed by Eq. (28) holds.

[1] L. Mandelstam, Ann. Phys. (Leipzig) **41**, 608 (1913).
[2] F. P. Buff, R. A. Lovett, and F. H. Stillinger, Jr., Phys. Rev. Lett. **15**, 621 (1965).
[3] R. Evans, Adv. Phys. **28**, 143 (1979).
[4] J. S. Rowlinson and B. Widom, *Molecular Theory of Capillarity* (Dover, Mineola, NY, 1982).
[5] S. A. Safran, *Statistical Thermodynamics of Surfaces, Interfaces and Membranes* (Addison-Wesley, New York, 1994).
[6] R. Loudon, Proc. R. Soc. London A **372**, 275 (1980).
[7] M. Grant and R. C. Desai, Phys. Rev. A **27**, 2577 (1983).
[8] F. Family and T. Vicsek, *Dynamics of Fractal Surfaces* (World Scientific, Singapore, 1991).
[9] A.-L. Barabasi and H. E. Stanley, *Fractal Concepts in Surface Growth* (Cambridge University Press, Cambridge, 1995).
[10] J. Krug and H. Spohn, in *Solids far from Equilibrium*, edited by C. Godreche (Cambridge University Press, Cambridge, 1991), p. 479.
[11] P. Meakin, Phys. Rep. **235**, 189 (1993).
[12] T. Halpin-Healy and Y. Zhang, Phys. Rep. **254**, 215 (1995).
[13] S. F. Edwards and D. R. Wilkinson, Proc. R. Soc. London **381**, 17 (1982).
[14] M. Kardar, G. Parisi, and Y.-C. Zhang, Phys. Rev. Lett. **56**, 889 (1986).
[15] E. G. Flekkoy and D. H. Rothman, Phys. Rev. Lett. **75**, 260 (1995).
[16] E. G. Flekkoy and D. H. Rothman, Phys. Rev. E **53**, 1622 (1996).
[17] E. M. Foard and A. J. Wagner, Phys. Rev. E **85**, 011501 (2012).
[18] S. G. Ayodele, F. Varnik, and D. Raabe, Phys. Rev. E **83**, 016702 (2011).
[19] A. J. Wagner and J. M. Yeomans, Phys. Rev. E **59**, 4366 (1999).
[20] Z. Shou and A. Chakrabarti, Phys. Rev. E **61**, R2200 (2000).
[21] A. J. Bray, A. Cavagna, and R. D. M. Travasso, Phys. Rev. E **64**, 012102 (2001).
[22] A. J. Bray, A. Cavagna, and R. D. M. Travasso, Phys. Rev. E **65**, 016104 (2001).
[23] D. G. A. L. Aarts and H. N. W. Lekkerkerker, J. Fluid. Mech. **606**, 275 (2008).
[24] M. Grant, Phys. Rev. B **37**, 5705 (1988).
[25] F. W. Starr, S. T. Harrington, B. M. Boghosian, and H. E. Stanley, Phys. Rev. Lett. **77**, 3363 (1996).
[26] J. Zittartz, Phys. Rev. **154**, 154 (1967).
[27] H. W. Diehl, D. M. Kroll, and H. Wagner, Z. Phys. B **36**, 329 (1980).
[28] R. Evans, Mol. Phys. **42**, 1169 (1981).
[29] J. Stecki, J. Chem. Phys. **108**, 3788 (1998).
[30] F. Sedlmeier, D. Horinek, and R. R. Netz, Phys. Rev. Lett. **103**, 136102 (2009).
[31] E. M. Blokhuis, J. Chem. Phys. **130**, 014706 (2009).
[32] U.-S. Jeng, L. Esibov, L. Crow, and A. Steyerl, J. Phys.: Condens. Matter **10**, 4955 (1998).
[33] A. Madsen, T. Seydel, M. Sprung, C. Gutt, M. Tolan, and G. Grübel, Phys. Rev. Lett. **92**, 096104 (2004).
[34] J. L. Harden, H. Pleiner, and P. A. Pincus, J. Chem. Phys. **94**, 5208 (1991).
[35] J. Jaeckle and K. Kawasaki, J. Phys.: Condens. Matter **7**, 4351 (1995).
[36] M. Thiebaud and T. Bickel, Phys. Rev. E **81**, 031602 (2010).
[37] V. Levich, *Physicochemical Hydrodynamics* (Prentice Hall, New York, 1962).
[38] M. A. Bouchiat and J. Meunier, J. de Phys. **33**, C1 (1972).
[39] S. Mora and J. Daillant, Eur. J. Phys. B **27**, 417 (2002).
[40] B. U. Felderhoff, Physica A **48**, 541 (1970).
[41] M. A. Bouchiat and J. Meunier, J. de Phys. **35**, 847 (1974).
[42] K. Falk and K. Mecke, J. Phys.: Condens. Matter **23**, 184103 (2011).
[43] A. J. C. Ladd, J. Fluid Mech. **271**, 285 (1994).
[44] R. Adhikari, K. Stratford, M. E. Cates, and A. J. Wagner, Europhys. Lett. **71**, 473 (2005).
[45] B. Dünweg, U. D. Schiller, and A. J. C. Ladd, Phys. Rev. E **76**, 036704 (2007).
[46] M. Gross, R. Adhikari, M. E. Cates, and F. Varnik, Phys. Rev. E **82**, 056714 (2010).
[47] M. Gross, M. E. Cates, F. Varnik, and R. Adhikari, J. Stat. Mech. (2011) P03030.
[48] M. Gross and F. Varnik, Phys. Rev. E **85**, 056707 (2012).
[49] M. R. Swift, W. R. Osborn, and J. M. Yeomans, Phys. Rev. Lett. **75**, 830 (1995).
[50] M. R. Swift, E. Orlandini, W. R. Osborn, and J. M. Yeomans, Phys. Rev. E **54**, 5041 (1996).
[51] R. Benzi, S. Succi, and M. Vergassola, Phys. Rep. **222**, 145 (1992).
[52] D. Raabe, Model. Simul. Mater. Sci. Eng. **12**, R13 (2004).
[53] S. Succi, *The Lattice Boltzmann Equation for Fluid Dynamics and Beyond* (Oxford University Press, Oxford, 2001).
[54] L. D. Landau and E. M. Lifshitz, *Fluid Mechanics* (Pergamon, Oxford, 1959).

[55] J. M. O. de Zarate and J. V. Sengers, *Hydrodynamic Fluctuations in Fluids and Fluid Mixtures* (Elsevier, New York, 2006).
[56] P. C. Hohenberg and B. I. Halperin, Rev. Mod. Phys. **49**, 435 (1977).
[57] J. S. Langer and L. A. Turski, Phys. Rev. A **8**, 3230 (1973).
[58] D. M. Anderson, G. B. McFadden, and A. A. Wheeler, Annu. Rev. Fluid. Mech. **30**, 139 (1998).
[59] P. M. Chaikin and T. C. Lubensky, *Principles of Condensed Matter Physics* (Cambridge University Press, Cambridge, 1995).
[60] D. Jamet, O. Lebaigue, N. Coutris, and J. M. Delhaye, J. Comp. Phys. **169**, 624 (2001).
[61] E. M. Blokhuis and D. Bedeaux, J. Chem. Phys. **97**, 3576 (1992).
[62] M. P. A. Fisher and M. Wortis, Phys. Rev. B **29**, 6252 (1984).
[63] B. Z. Shang, N. K. Voulgarakis, and J.-W. Chu, J. Chem. Phys. **135**, 044111 (2011).
[64] V. Yermakou and S. Succi, Physica A **391**, 4557 (2012).
[65] O. Behrend, R. Harris, and P. B. Warren, Phys. Rev. E **50**, 4586 (1994).
[66] P. Lallemand and L.-S. Luo, Phys. Rev. E **61**, 6546 (2000).
[67] L. A. Turski and J. S. Langer, Phys. Rev. A **22**, 2189 (1980).
[68] X. Shan and H. Chen, Phys. Rev. E **49**, 2941 (1994).
[69] R. Zhang, X. He, and S. Chen, Comp. Phys. Comm. **129**, 121 (2000).